Regeneration of near-wall turbulence structures

By James M. Hamilton, John Kim AND Fabian Waleffe

1. Motivation and objectives

A remarkable feature of the coherent structures observed in turbulent shear flows is that these structures are self-regenerating. Individual structures may break up or decay, but their presence ensures the creation of subsequent structures. It is through a continuous cycle of generation and regeneration that the turbulence is sustained. In the near-wall region, the principal structures are low- and high-speed streaks and streamwise vortices, and these structures have a characteristic spanwise "wavelength" of about 100 ν/u_τ ($u_\tau = \sqrt{\tau_w/\rho}$ is the friction velocity and τ_w is the shear stress at the wall). The mechanisms involved in the regeneration process, including those which govern the spanwise spacing of the streaks, have, however, been tremendously difficult to determine. Many studies have focused on the kinematics of coherent structures (*e.g.* Kline, *et al.*, 1967, Robinson, 1991), from which the dynamics of regeneration can only be inferred. Direct examination of the flow dynamics in a fully turbulent flow is complicated by the random distribution of the coherent structures in space and time and by the presence of additional structures which may not be essential components of the regeneration process.

Several investigators have avoided these complications by studying simplified flows and, often, by considering only part of the regeneration process. Jiménez and Moin (1991), for example, used direct numerical simulation to study turbulence in a channel flow at Reynolds numbers of 2000 to 5000, simplifying the problem by considering a computational domain in which the streamwise and spanwise dimensions were near the minimum values required to sustain turbulence. The boundary conditions in these directions were periodic, and the flow thus consisted of a doubly periodic array of identical cells. Despite the constraint imposed by the small size of the computational domain, various statistical measures (mean streamwise velocity profile, Reynolds stresses, turbulence intensities) and turbulence structures (sublayer streaks, streamwise vortices, near-wall shear-layers) in the near-wall region closely matched those observed by other investigators.

The origin of the streamwise vortices was addressed by Jang, Benney & Gran (1986) who employed "direct resonance" theory to explain the observed spanwise spacing of the vortices and the accompanying streaks. The direct resonance mechanism produces rapid growth of oblique wall-normal vorticity modes, but applies only to modes which satisfy a resonance condition, and thus provides a scale selectivity. These wall-normal vorticity modes can then interact to form streamwise vortices and streaks of the correct spacing. Subsequently, however, Waleffe & Kim (1991) examined direct resonance and noted that some nonresonant modes were amplified more than the resonant modes, eliminating any scale selection due to the resonance mechanism. Furthermore, they found that the creation of streamwise vortices by

the interactions of oblique modes was dominated by the interactions of the wall-normal velocity modes rather than the wall-normal vorticity modes assumed in the direct resonance theory.

Jiménez and Moin addressed the issue of streak spacing when they noted that turbulence could not be sustained in their plane channel flow simulations if the spanwise dimension of the computational domain was less than the normally observed streak spacing, about 100 wall units, even though the flow Reynolds number, based on half the separation of the channel walls, was 2000 to 5000. This is a fascinating result since reducing the width not only eliminated the streaks, but the turbulence, too. The streaks (or whatever produces them) are not mere artifacts, but essential features of turbulent flow. Waleffe & Kim observed that at 100 wall units, the width of the channel is much less than the wall separation, and that the Reynolds number might more appropriately be based on the spanwise dimension. Indeed, the characteristic spanwise spacing, λ_z, when expressed in wall units, $u_\tau \lambda_z/\nu$, is like a Reynolds number, and the value of 100 may be regarded as the critical Reynolds number for sustained turbulence. This led Waleffe & Kim to conjecture that the preferred spanwise spacing is set by the entire process of self-regeneration rather than by any of the individual mechanisms that constitute the process. They went on to show that the critical Reynolds number obtained from the streak spacing, after conversion to the conventional flow Reynolds number, gives the correct critical values for plane Poiseuille and plane Couette flows.

The present study is an examination of the regeneration mechanisms of near-wall turbulence and an attempt to investigate the critical Reynolds number conjecture of Waleffe & Kim. The basis of this study is an extension of the "minimal channel" approach of Jiménez and Moin which emphasizes the near-wall region and further reduces the complexity of the turbulent flow. Reduction of the flow Reynolds number to the minimum value which will allow turbulence to be sustained has the effect of reducing the ratio of the largest scales to the smallest scales or, equivalently, of causing the near-wall region to fill more of the area between the channel walls. In addition, since each wall may have an active near-wall region, half of the channel is always somewhat redundant. If a plane Couette flow is instead chosen as the base flow, this redundancy is eliminated: the mean shear of a plane Couette flow has a single sign, and at low Reynolds numbers, the two wall regions share a single set of structures. A minimal flow with these modifications possesses, by construction, the strongest constraints which allow sustained turbulence, producing a greatly simplified flow in which we can examine the regeneration process.

2. Accomplishments

2.1 Numerical method and flow geometry

The direct numerical simulation results presented here were obtained using the pseudo-spectral channel flow code of Kim, Moin & Moser (1987) modified to simulate plane Couette flow and using a third-order Runge-Kutta time advancement for the convective terms rather than the original Adams-Bashforth. Dealiased Fourier

expansions are used in the streamwise (x) and spanwise (z) directions, and Chebychev polynomials are used in the wall-normal (y) direction. Boundary conditions are periodic in x and z, and the no-slip condition is imposed at the walls. The mean streamwise pressure gradient is zero, and the flow is driven by the motion of the walls. The flow velocities in the x, y, and z directions are u,v, and w, respectively. The Fourier transforms of the velocities are "hatted" and are functions of the streamwise wavenumber, k_x, the spanwise wavenumber, k_z, and the untransformed y-coordinate, *e.g.* $\hat{u}(k_x, y, k_z)$. The fundamental streamwise and spanwise wavenumbers are $\alpha \equiv 2\pi/L_x$ and $\beta \equiv 2\pi/L_z$. Dimensional quantities are denoted by an asterisk superscript. No superscript is used for quantities non-dimensionalized by outer variables: half the wall separation, h^*, and the wall velocity, U_w^*. A plus superscript is used for quantities non-dimensionalized by wall variables: kinematic viscosity, ν, and friction velocity, $u_\tau = \sqrt{\tau_w/\rho}$. The flow Reynolds number is based on outer variables: Re$= U_w^* h^*/\nu$. The computational grid is $16 \times 33 \times 16$ in x, y, and z. Because of the small computational domain, u_τ varies with time, but the resolution in wall units lies in the range $\Delta x^+ = 10.8$–13.0, $\Delta z^+ = 7.4$–8.9, and $\Delta y^+ = .15$–$.18$ near the wall, and 3.1–3.7 at the center of the channel.

2.2 Regeneration cycle

The first step in the study of the regenerative cycle of near-wall turbulent structures was to determine the minimum Reynolds number and minimum dimensions of the periodic domain of a plane Couette flow. Computations for Reynolds number minimization began with random initial conditions at Re=625, a value known to produce sustained turbulence. The resulting flow was allowed to develop in time, the Reynolds number reduced, and the flow once again allowed to evolve. The Reynolds number was reduced in this manner to Re=500 and 400, with turbulence no longer sustained at Re=300. The domain size was minimized in a similar fashion with reductions first in the spanwise dimension, L_z, then in the streamwise dimension, L_x. Finally, the parameter values selected are $L_x = 1.75\pi$ and $L_z = 1.2\pi$ at Re=400. Turbulence could be sustained at slightly lower L_x and L_z; however, these values were chosen because they produce a flow which is better suited to the present study, as discussed below.

The flow realized in this small domain is ideal for examining the turbulence regeneration mechanisms. Much of the randomness in the location of the turbulence structures is eliminated, and regeneration occurs temporally in a well defined, quasi-cyclic process. The general characteristics of the flow over one complete regeneration cycle can be seen in Figure 1. This is a plot of streamwise (u) velocities in the x-z plane midway between the walls at various times. At the upper left, the flow can be seen to have little x-dependence, and strong streak-like structures dominate the flow. As time increases, the x-dependence increases, with the streak becoming "wavy" and then breaking down. "Break down" means the production of smaller scale features and loss of definition of the streak, particularly near the walls. Finally, at the lower right, a well-defined, nearly x-independent streak has been regenerated, and the cycle is ready to repeat.

Because a spectral method is used in these simulations, Fourier decomposition is

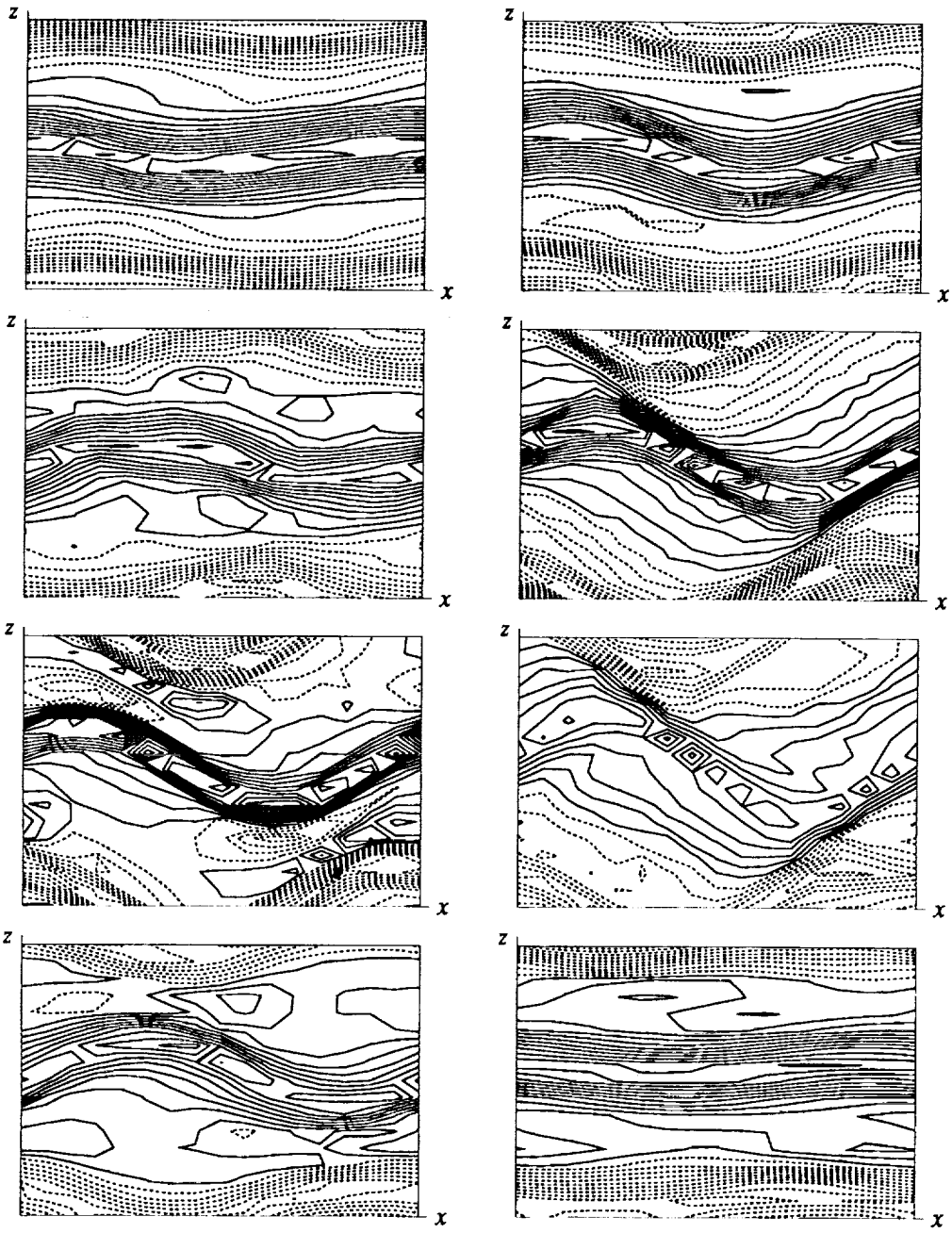

FIGURE 1. Iso-contours of u-velocity in x-z plane centered between walls, solid contours positive, dashed contours negative. Contour interval 0.032. Time increases from left to right, top to bottom. Times are: $t = 757.5$, $t = 764.8$, $t = 772.0$, $t = 777.8$, $t = 783.0$, $t = 794.1$, $t = 808.2$, $t = 830.2$.

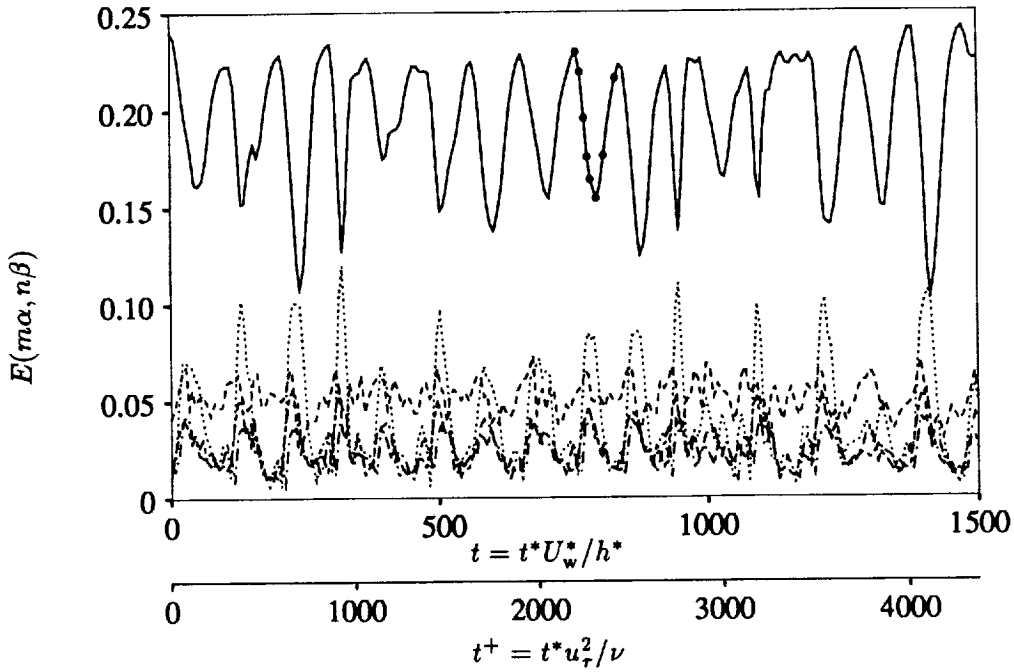

FIGURE 2. Modal energy over many regeneration cycles. Solid circles correspond to times of Figure 1. ——— , $E(0,\beta)$; – – – – , $E(0,2\beta)$; - - - - - - , $E(\alpha,0)$; — — — , $E(\alpha,\beta)$; - — - — - , $E(\alpha,2\beta)$.

a natural means to study the regeneration cycle. The modal kinetic energy is given by

$$E(m\alpha, n\beta) \equiv \int_{-1}^{1} \left[\hat{u}^2(m\alpha, y, n\beta) + \hat{v}^2(m\alpha, y, n\beta) + \hat{w}^2(m\alpha, y, n\beta)\right] dy, \quad (1)$$

and Figure 2 is a plot of this energy in various modes over many cycles. The cyclic nature of the flow particularly apparent in the $(0,\beta)$ and $(\alpha,0)$ modes of Figure 2. Though $E(0,\beta)$ is the energy from all three modal velocity components, the dominant contribution is from $\hat{u}(0,y,\beta)$, the fundamental-in-z, x-independent streamwise velocity mode, *i.e.* the streaks. The flow of Figure 1 is a single cycle of the flow of Figure 2, and the corresponding times are marked. Note the decrease and then increase in $E(0,\beta)$ as the flow passes from small x-dependence to large x-dependence and back again. The period of the regeneration cycle is slightly less than 100, based on 16 cycles in 1500 time units in Figure 2. This is approximately the same period observed by Jiménez and Moin in their minimal channel flow at higher Reynolds number, though their channel flow and the present plane Couette flow have slightly different time normalizations. The regeneration cycle can be divided roughly into two phases, each with a duration of about 50 time units: streak formation, where $dE(0,\beta)/dt > 0$, and streak breakdown, where $dE(0,\beta)/dt < 0$.

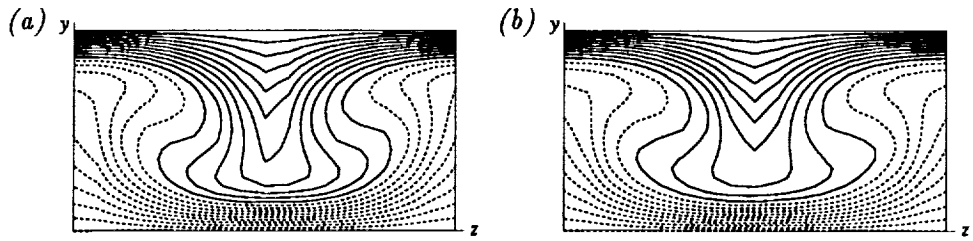

FIGURE 3. Streaks (u-velocity) due to *(a)* streamwise vortices only, at peak of $E(0,\beta)$ response, and *(b)* full simulation. Velocity field in physical space is obtained by inverse Fourier transform in x and z of the $k_x = 0$ modes only. Dashed lines are negative contours. Contour interval, 0.2.

2.3 Streak formation

It is usually argued that streamwise vortices generate the low- and high-speed streaks observed in the near-wall region (*e.g.* Swearingen and Blackwelder, 1987; Waleffe & Kim, 1991). In the present study, various methods of visualization of the flow give clear evidence of the presence of streamwise vortices, and it is desirable to verify that these vortices can not only generate streaks, but generate the observed streaks.

In Figure 1 the streaks remain apparent for most of the regeneration cycle. Nearer the walls, however, the streaks are most clearly defined when the flow is nearly x-independent at times corresponding to peaks in the energy of the $(0,\beta)$ mode. Therefore, in studying streak formation, it is useful to focus on the x-independent ($k_x = 0$) modes. To verify that the vortices produce the streaks, the velocity field at $t = 758$, corresponding to a peak in $E(0,\beta)$, is taken as the initial condition for a model simulation. This initial condition is modified by zeroing all but the $k_x = 0$ modes and zeroing all the $\hat{u}$ modes *except* the mean streamwise velocity mode, $\hat{u}(0,y,0)$. In addition, the $\hat{v}(0,y,n\beta)$ and $\hat{w}(0,y,n\beta)$ modes are held fixed ("frozen") during the model simulation. The energy in the $(0,\beta)$ mode peaks after about 50 time units, the same time scale as in the full simulation, and the resulting streaks are virtually identical to the streaks from the full simulation at $t = 758$, as shown in Figure 3. A similar model simulation with an initially linear $\hat{u}(0,y,0)$ velocity profile indicates that the mean velocity profile is due principally to the streamwise vortices as well.

2.4 Streak breakdown

It is often argued that breakdown occurs due to an instability (*e.g.* Swearingen and Blackwelder, 1987), and the "waviness" that develops in the high- and low-speed streaks in Figure 1 is certainly reminiscent of an instability process. In order to determine whether breakdown is due to an instability in the present case, the growth or decay of small amplitude, spatially random fluctuations in an otherwise x-independent flow was examined. The initial conditions for a model simulation were taken from the flow of Figures 1 and 2 at time $t = 758$, corresponding to a peak in $E(0,\beta)$. The $k_x = 0$ modes of $\hat{u}$, $\hat{v}$, and $\hat{w}$ (*i.e.* the x-independent modes)

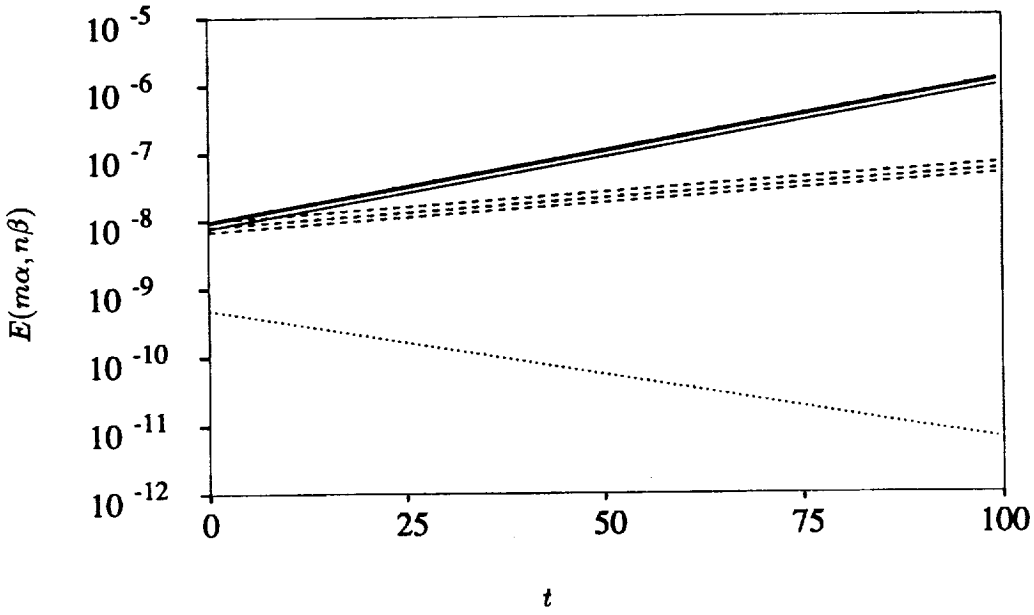

FIGURE 4. Linear stability of $k_x = 0$ modes of flow from full simulation at $t = 757.5$: ——— , $(\alpha, 0)$, (α, β) and $(\alpha, 2\beta)$ modes; – – – – , $(2\alpha, 0)$, $(2\alpha, \beta)$ and $(2\alpha, 2\beta)$ modes; - - - - - - , $(3\alpha, 0)$ modes.

were retained unaltered, and random perturbations, uniformly distributed from zero to 10^{-6}, were placed in all remaining Fourier modes. The $k_x = 0$ modes were "frozen", and the perturbations were allowed to evolve normally. This procedure is much like that used to observe the development of streaks in the previous section, except that here both the cross-flow and the streaks are frozen, and it is the growth of perturbations in the x-dependent modes that are of interest. The small initial perturbation amplitudes were chosen in order to study the linear stability of the flow. If the base flow is unstable, the fastest growing instability mode would be expected to dominate after sufficient time, and in general, this instability mode will consist of many spanwise Fourier modes. The results of this simulation show that the streaks are indeed linearly unstable. The growth in energy of the most unstable modes is shown in Figure 4. For purposes of this plot, the α and 2α instability modes obtained from the simulation were normalized to have approximately the same initial amplitude. Note that the various spanwise Fourier modes that contribute to each instability mode grow in energy at the same rate.

Comparison of the linear stability results to the full simulation shows some differences, but these are to be expected since breakdown is clearly a nonlinear process. The waviness that develops during actual breakdown is not really a "mode"; for instance, $E(\alpha, 0)$, $E(\alpha, \beta)$ and $E(\alpha, 2\beta)$ do not grow together as a single instability mode in Figure 2 as they do in Figure 4. In addition, the time scale of the linear

instability is too long, with $E(\alpha,0)$ in Figure 2 growing by nearly an order of magnitude in less than 20 time units during breakdown, while the α instability mode in the linear simulation of Figure 4 requires nearly 50 time units. The linear approach matches the rapid growth rates of the simulation only during the initial, transient phase. The principal limitation of the linear approach is that the flow we are trying to analyze evolves on the same time scale as the instability. Comparison of the shapes of the linear α-modes to the α-modes obtained in the full simulation (results not shown here) again show some differences but are surprisingly good considering the limitations of the linear approach.

2.5 Streamwise vortex regeneration

The regeneration of turbulence structures as discussed so far consists of a continuous cycle of streak formation and breakdown. Streak formation was shown to be the result of momentum redistribution by streamwise vortices, but this raises the question of the origin of the streamwise vortices.

The streamwise vortices persist throughout the regeneration cycle of Figure 1 and during the many regeneration cycles of Figure 2. It can be shown that streamwise vortices in a strictly x-independent flow will eventually decay: there is no mechanism for the vortices to extract energy directly from the mean flow. Therefore, the x-dependent modes must somehow augment the streamwise vortices if the regeneration cycle is to continue. Though not shown here, plots of the velocity field in the cross-flow (y–z) plane indicate that this augmentation takes place primarily during streak breakdown, when the x-dependence of the flow is greatest. For the cycle of Figure 1, the strength of the streamwise vortices has just begun to increase by the time of the third panel, $t = 772$. The modal interactions which cause this augmentation can be studied by a model simulation using the flow field at $t = 772$ as an initial condition, again with selective alteration of various Fourier modes. In this case, all modes are set to zero except the mean, $\hat{u}(0,y,0)$,and the α-modes: $\hat{u}$, $\hat{v}$, and $\hat{w}$ of $(\alpha,y,n\beta)$ (for all n). In addition, the α-modes are frozen. With this initial condition, streamwise vortices quickly appear, and these vortices then produce streaks, as would be expected. If the α-modes are then "unfrozen", the flow *immediately* begins to follow the regenerative cycle normally observed. This process is shown in Figure 5. Up to $t = 34.9$, the α-modes are frozen, and $E(0,\beta)$ is seen to rapidly increase. After $t = 34.9$ (the heavy vertical line), the α-modes are unfrozen. The energy in the $(0,\beta)$ mode decreases slightly as breakdown due to the α-modes continues, followed by streak regeneration and another cycle. This approach shows that it is the α-modes which regenerate the streamwise vortices but does not reveal the dynamics of the process. The dynamics are most easily studied by an examination of the evolution of streamwise vorticity.

To compare the contributions of the individual nonlinear terms of the vorticity equation over time, it is easiest to consider

$$\frac{\partial|\hat{\omega}_x|^2}{\partial t} = \hat{\omega}_x^\dagger \frac{\partial \hat{\omega}_x}{\partial t} + \hat{\omega}_x \frac{\partial \hat{\omega}_x^\dagger}{\partial t} \tag{2}$$

(where the † superscript represents the complex conjugate), since this quantity is

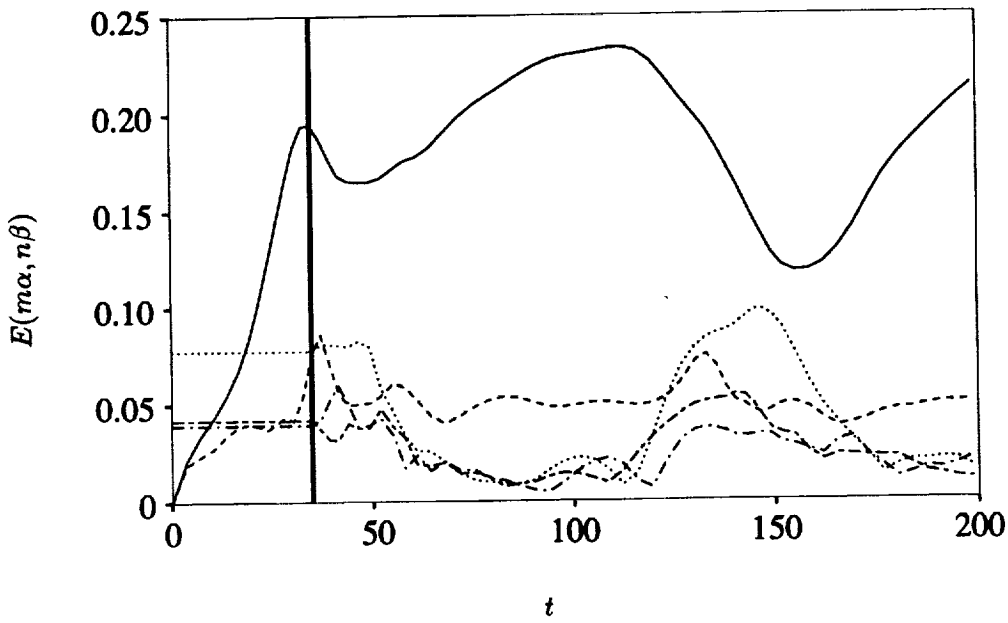

FIGURE 5. Regeneration of streamwise vortices from $k_x = \alpha$ modes, and subsequent reversion to regeneration cycle. Initially conditions: $k_x = \alpha$ modes from full simulation at $t = 772.0$, and all $k_x = 0$ modes zero except $\hat{u}(0, y, 0)$. The $k_x = \alpha$ modes are frozen until $t = 34.9$ (heavy line), and thereafter all modes are free to evolve. Modes plotted same as Figure 2.

positive at y-locations where the existing streamwise vorticity is being augmented and negative where the vorticity is being reduced. The contributions of each term at the y-location of the maximum magnitude of the term are plotted in Figure 6. One might hope, for simplicity, that only a single term in the vorticity equation would be dominant. In fact, one term has about twice the amplitude of any other,

$$-\hat{\omega}_x^\dagger(0,\beta)\left[\hat{v}(\alpha,\beta)\frac{\partial\hat{\omega}_x(-\alpha,0)}{\partial y}+\hat{v}(-\alpha,\beta)\frac{\partial\hat{\omega}_x(\alpha,0)}{\partial y}\right]+C.C., \tag{3a}$$

but four other terms are significant,

$$\hat{\omega}_x^\dagger(0,\beta)\left[\hat{\omega}_y(\alpha,0)\frac{\partial\hat{u}(-\alpha,\beta)}{\partial y}+\hat{\omega}_y(-\alpha,0)\frac{\partial\hat{u}(\alpha,\beta)}{\partial y}\right]+C.C. \tag{3b}$$

$$-\hat{\omega}_x^\dagger(0,\beta)\left[\hat{w}(\alpha,0)\frac{\partial\hat{\omega}_x(-\alpha,\beta)}{\partial z}+\hat{w}(-\alpha,0)\frac{\partial\hat{\omega}_x(\alpha,\beta)}{\partial z}\right]+C.C. \tag{3c}$$

$$-\hat{\omega}_x^\dagger(0,\beta)\left[\hat{u}(\alpha,\beta)\frac{\partial\hat{\omega}_x(-\alpha,0)}{\partial x}+\hat{u}(-\alpha,\beta)\frac{\partial\hat{\omega}_x(\alpha,0)}{\partial x}\right]+C.C. \tag{3d}$$

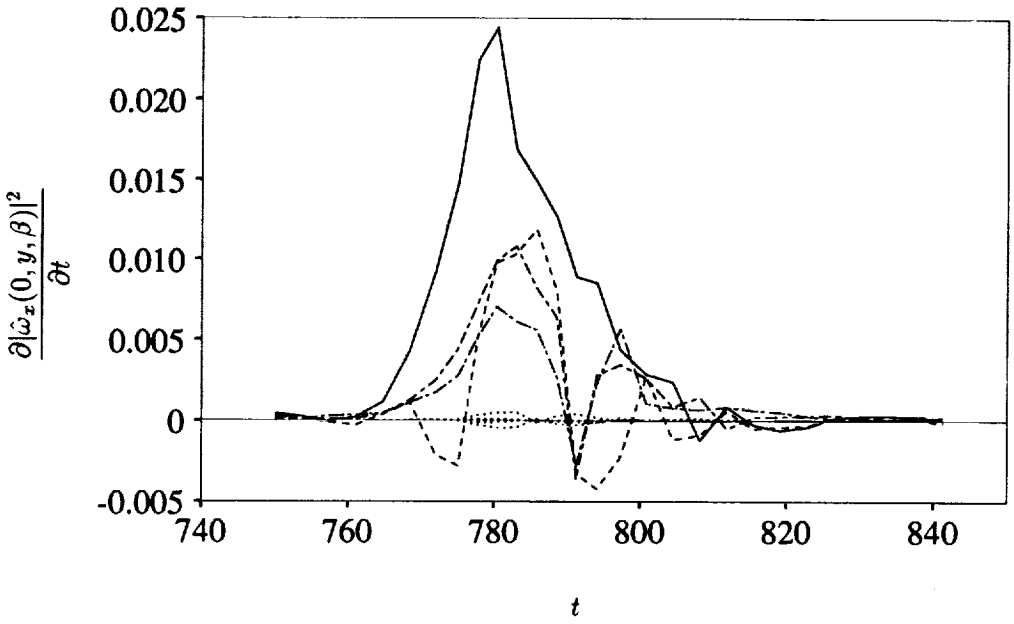

FIGURE 6. Contributions of various terms to $\partial|\hat{\omega}_x(0,y,\beta)|^2/\partial t$ at y-locations corresponding to maximum amplitudes. ———, Expression 3a; – – – –, Expression 3b; — — —, Expression 3c; -·-·-, Expressions 3d and 3e; ------, all other interactions.

$$\hat{\omega}_x^\dagger(0,\beta)\left[\hat{\omega}_x(\alpha,0)\frac{\partial\hat{u}(-\alpha,\beta)}{\partial x}+\hat{\omega}_x(-\alpha,0)\frac{\partial\hat{u}(\alpha,\beta)}{\partial x}\right]+C.C. \qquad (3e)$$

The y-dependence has been suppressed, and the $C.C.$ are the complex conjugates. Expressions 3d and 3e turn out to be identical for the $(0,\beta)$ mode, thus there are only four dominant curves in Figure 6. This vortex regeneration process is repeated for every breakdown event. The importance of vortex regeneration is particularly evident in the discussion of the next topic, the spanwise spacing of streaks.

2.6 Spanwise spacing of structures

Jiménez and Moin (1991) found that when the spanwise dimension of their computational domain was less than the typically observed spanwise spacing of the streaks, turbulence could not be sustained. As discussed in §1, this led Waleffe & Kim (1991) to conjecture that the streak spacing is determined by the entire self-regeneration process. The regeneration process has been examined in some detail in previous sections, and the techniques used to investigate regeneration can now be used to address the issue of the spanwise spacing of near-wall structures.

The first step is to reduce the dimensions of the computational domain just enough that turbulence is sustained through several regeneration cycles but ultimately decays. Then we can study the details of the flow to determine which part(s)

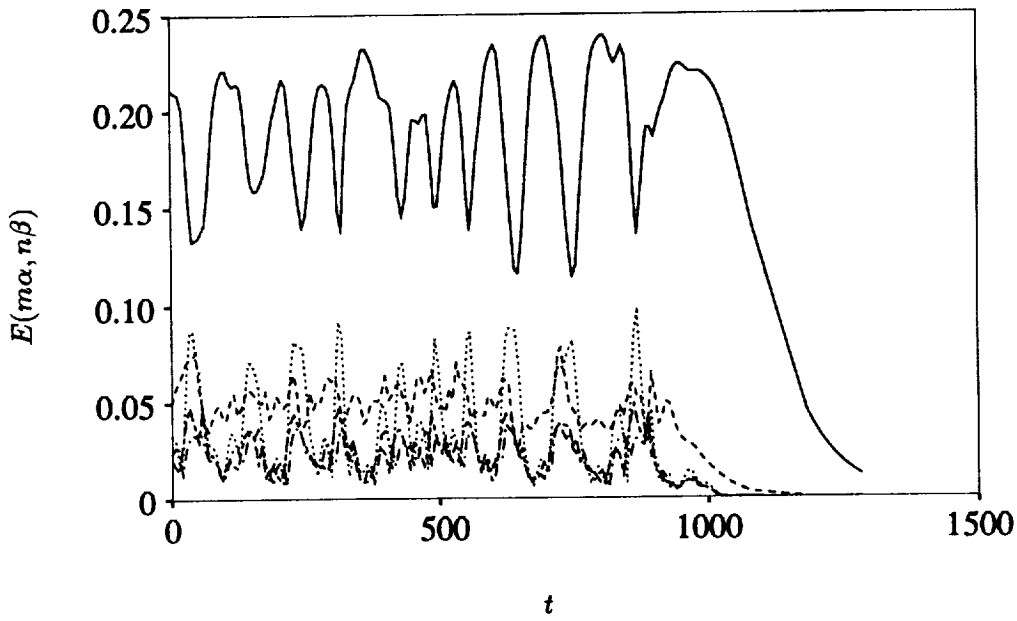

FIGURE 7. Modal energy over many regeneration cycles of an unsustainable turbulent flow: ——— , $E(0,\beta)$; – – – – , $E(0,2\beta)$; - - - - - - , $E(\alpha,0)$; — – — , $E(\alpha,\beta)$; — - — - , $E(\alpha,2\beta)$.

of the regeneration cycle is disrupted. The modal energies for such a flow are plotted in Figure 7. The spanwise dimension of the flow is $L_z = 1.1\pi$, or $L_z^+ = 109.2$ to 126.1 (where L_z^+ is based on u_τ during the early part of the simulation before the turbulence begins to decay). The streamwise dimension is $L_x = 1.6\pi$, and the same Reynolds number, 400, is used. This flow was obtained by first reducing the spanwise dimension of a sustainable turbulent flow and then the streamwise dimension. Turbulence can be sustained in this channel if L_x is increased, but the cycle is very chaotic. Turbulence can also be sustained if L_z is increased.

The regeneration of the streamwise vortices for the unsustainable flow is plotted in Figure 8 for the last few cycles of Figure 7. Vortex regeneration takes place during each streak breakdown event, between $t = 600$ and $t = 900$, but the amount of streamwise vorticity added to the flow decreases with each succeeding cycle. Finally, for $t > 900$, the flow simply decays with no breakdown and no corresponding vortex regeneration.

As the production of streamwise vorticity decreases, the average strength of the streamwise vortices decreases. There is little visible difference in the streaks produced by these weaker vortices, but the instability of the streaks is dramatically reduced as the strength of the streamwise vortices goes down (results not shown here). The flow actually becomes linearly stable by $t = 1000$, and breakdown does not occur.

The computations of this section indicate that the spanwise wavelength of the

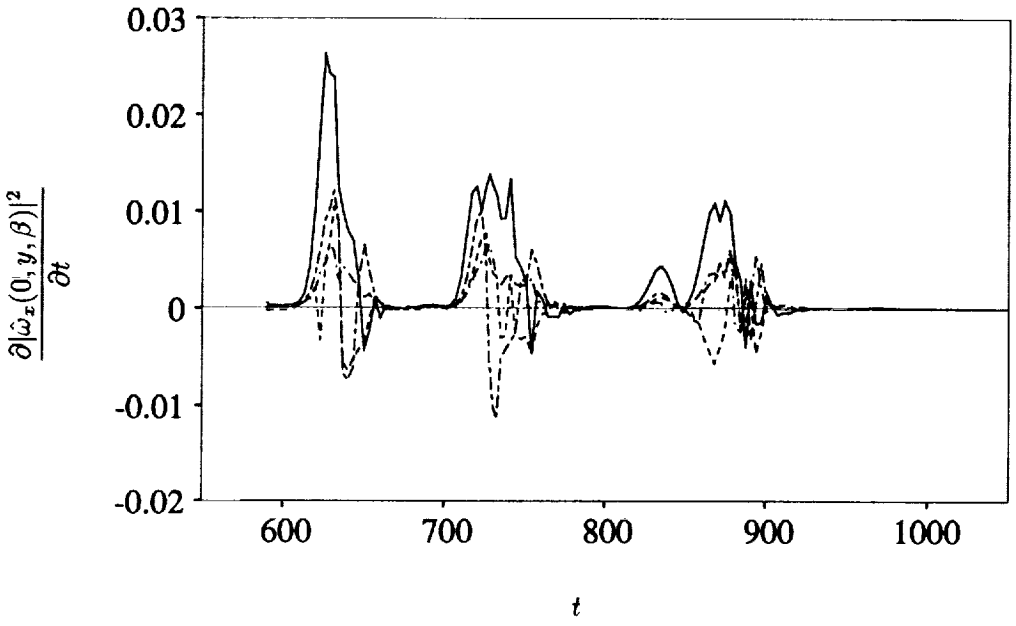

FIGURE 8. Contributions of various terms to $\partial|\hat{\omega}_x(0,y,\beta)|^2/\partial t$ at y-locations corresponding to maximum amplitudes in an unsustainable turbulent flow: ——— , Expression 3a; – – – – , Expression 3b; — – — , Expression 3c; - – - – - , Expressions 3d and 3e; - - - - - - , all other interactions.

near-wall structures is determined by the minimum wavelength required by the regeneration process. This would seem to confirm the conjecture by Waleffe & Kim that this minimum wavelength is set by the entire regeneration process rather than any individual element of regeneration. When the computational domain is too narrow, turbulence decays because the streamwise vortices are inadequately regenerated during each cycle. Vortex regeneration, in turn, depends on the interactions of the α modes produced during breakdown, and breakdown depends on the stability of the streaks produced by the streamwise vortices. This, of course, returns us to the starting point because the streamwise vortices depend on the vortex regeneration of the previous cycle. Ultimately, turbulence decayed in the flow of Figure 7 because breakdown did not occur. But, each step in the regeneration process was progressively weaker for several cycles before the final decay, and thus it was the entire regeneration process that was unsustainable in this flow.

3. Future plans

The results presented here give a fairly complete picture of the regeneration process for near-wall turbulence structures in a minimal domain, but the real objective, of course, is to relate these observations to the near-wall structures in a larger domain at higher Reynolds numbers. Thus, the major element of future work is to examine these processes in full-scale turbulence. Rather than move directly to an

examination of existing databases, however, the robustness of the observed mechanisms will first be checked by a step-by-step increase in the dimensions and Reynolds numbers of the minimal domain.

Some of the details of the present work will also be examined further. For instance, in the work relating to the minimum spanwise spacing of the streaks in §2.6, the length of the domain, L_x, has some effect on whether turbulence is sustained. This dimension will be significantly increased in some future computations so that the streamwise wavenumber of the most unstable modes will be selected by the flow rather than by the choice of box size.

The quasi-cyclic nature of the regeneration cycle also suggests some application of these results to turbulence control. Since breaking the cycle at any point may be sufficient to suppress turbulence, it would be useful to examine regeneration with the aim of implementing possible control schemes.

REFERENCES

JANG, P. S., BENNEY, D. J., & GRAN, R. L. 1986 On the origin of streamwise vortices in a turbulent boundary layer. *J. Fluid Mech.* **169,** 109-123.

JIMENEZ, J. & MOIN, P. 1991 The minimum flow unit in near-wall turbulence. *J. Fluid Mech.* **225,** 213-240.

KIM, J., MOIN, P. & MOSER, R. 1987 Turbulence statistics in fully developed channel flow at low Reynolds number. *J. Fluid Mech.* **177,** 133-166.

KLINE, S. J., REYNOLDS, W. C., SCHRAUB, F. A., & RUNSTADLER, P. W. 1967 The structure of turbulent boundary layers. *J. Fluid Mech.* **30,** 741.

ROBINSON, S. K. 1991 The Kinematics of Turbulent Boundary Layer Structure. *NASA TM-103859.*

SWEARINGEN, J. D. & BLACKWELDER, R. F. 1987 The growth and breakdown of streamwise vortices in the presence of a wall. *J. Fluid Mech.* **182,** 255.

WALEFFE, F. & KIM, J. 1991 On the origin of streaks in turbulent boundary layers. *Proceedings of the Eighth Symposium on Turbulent Shear Flows,* Technical University of Munich, Sept. 9-11.